Spatial Inhomogeneities and the Spectral Behavior of Atmospheric Aerosol Optical Depth over the Atlantic Ocean

SERGEY M. SAKERIN AND DMITRY M. KABANOV

Institute of Atmospheric Optics, Tomsk, Russia

(Manuscript received 16 November 2000, in final form 23 May 2001)

ABSTRACT

In this paper the results of investigations into atmospheric aerosol optical depth (AOD) over the Atlantic Ocean are discussed. The data were collected during five shipboard expeditions that took place between 1989 and 1996. Measurements were taken by a 0.37–4-μm multiwavelength sun photometer, specially designed for working conditions on board a ship. The analysis focuses on the spatial variability of atmospheric transparency and the spectral behavior of AOD in different oceanic areas. The genetic zoning of aerosol turbidity takes into account the influence of two factors: the type of continental aerosol and the character of airmass transport that dominates in a given latitudinal zone. The area selection by the genetic zoning method is further confirmed by the results of the ''sign'' classification based on the spatial distributions of AOD and the Ångström parameter. Statistical characteristics for different areas of the Atlantic are given. The mean values of AOD (0.55 μm) range from 0.08 to 0.38 and the mean Ångström parameters from 0.3 to 1.1. The spectral dependencies of AOD in the extended wavelength range (0.37–4 μm) are represented as the sum of two components related to the contribution of fine and coarse aerosols. It is noted that the largest spatial inhomogeneities of integral atmospheric transparency are caused by the aerosol component, and in most areas the coarse aerosol is a principal contributor to the extinction of radiation.

1. Introduction

It is well known that aerosols play an important role in atmospheric radiation transfer and radiation climatology (e.g., Kondratyev 1991; d'Almeida et al. 1991). Under cloudless conditions the inflow of solar radiation is determined by the total atmospheric transmission function $T^{\Sigma} = T^{A}T^{W}T^{X}T^{C}T^{R}$, which depends on the aerosol T^{A} and the water vapor T^{W} components, as well as on the transmission of other gases: $T^{C}T^{X}T^{R}$ (CO_2, O_3, Rayleigh scattering, etc.). An important feature of the main components T^{A} and T^{W} is that they are very sensitive to regional and synoptic variations. The contribution of other components can be treated as constant or calculated with a reasonable accuracy from modeled mean data for a particular season and latitudinal zone.

The continental network operations (Gushin 1988; Forgan et al. 1994) allowed us to obtain extensive empirical data to reveal the features of the spatial and temporal variability of the spectral and integral atmospheric transparency, aerosol optical depth (AOD), τ^{A}, and columnar water vapor. The knowledge of the optical characteristics of the oceanic atmosphere is less complete and reliable since it is based on scanty data from shipborne measurements and coastal stations data that are subject to continental influences. Judging from the review paper (Smirnov et al. 1995b), there were, in all, about 50 expeditions in the world's oceans that investigated AOD. In a majority of these expeditions the data were obtained during a few days or for a narrow spectral range (1–2 wavelengths). Even for the most visited area, such as the Atlantic Ocean, the total bulk of data is comparable to a 2-yr observation cycle at a single continental station. In this connection, let us dwell on the objective methodic shortcomings typical of marine studies of the atmospheric transparency.

First, the difficulty of onboard ship measurements leads to an even greater discontinuity of the observation series, as compared to ground-based measurements. If we estimate the degree of ''regularity'' as the ratio of the number of days of observation to the total period of measurement, then for the majority of investigations this value will be from 0.3 to 0.6. Second, the data obtained in the course of navigation are a cumulative result of the spatial and temporal variability of the atmospheric transparency. Last, individual marine investigations, contrary to uniform network observations, use different wavelength ranges and techniques to measure and calculate the τ^{A}. All these make it difficult to compare and generalize the isolated data of different expeditions.

Considering the problem of the spatial and variability

Corresponding author address: Dr. S. Sakerin, Institute of Atmospheric Optics, Tomsk 634050, Russia.
E-mail: sms@iao.ru

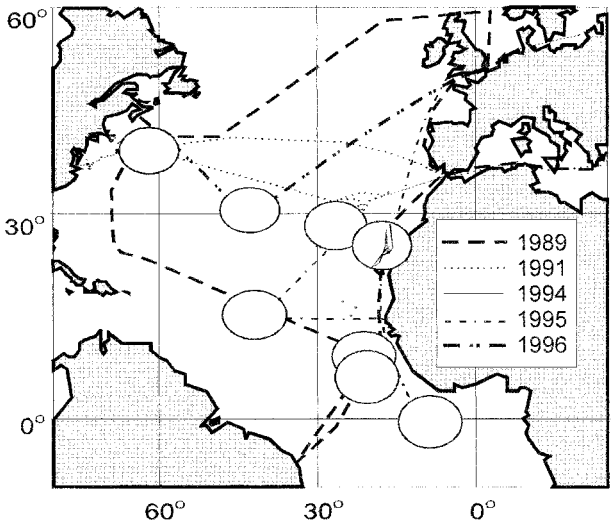

FIG. 1. The routes of five expeditions (sites of the most intensive observations are circled).

of the atmospheric transparency over the ocean, one cannot fail to mention the results of global spaceborne observations by means of the Advanced Very High Resolution Radiometers (AVHRR, the moderate resolution imaging spectroradiometers, and the Sea-viewing Wide Field-of-view Sensor (e.g., Mishchenko et al. 1999; Swap et al. 1996; Kaufman et al. 1997; Tanre et al. 1997). Though these investigations are important and promising, the error of reconstructing τ^A from the satellite data amounts to 0.03–0.05 (Rao et al. 1989; Ignatov et al. 1995; Tanre et al. 1997), and the results are usually related to one wavelength. Thus they cannot reveal the regional and meteorological features in the spectral behavior of AOD.

The most detailed shipborne investigations of τ^A were carried out in the 1970s through the 1980s by two groups: Barteneva et al. (1991) and Shifrin et al. (Shifrin et al. 1980; Volgin et al. 1988; Yershov et al. 1990; Villevalde et al. 1994; Smirnov et al. 1995a; etc.). Recent multiwave investigations of τ^A_λ in different regions were conducted by a number of authors (Tomasi et al. 1982; Hoyningen-Huene et al. 1987; Hoppel et al. 1990; Reddy et al. 1990; Moorthy et al. 1997; Satheesh et al. 1998; etc.). The cited papers discuss various properties and dependencies of τ^A_λ, but an analysis of the spatial variability of transparency over large areas was left beyond their scope.

Long-term optical investigations of the atmosphere were carried out by the authors of this paper over a significant portion of the Atlantic Ocean in 1989–96. These investigations, to some extent, fill the gap in our knowledge of the transparency of the marine atmosphere (Sakerin et al. 1991; Sakerin et al. 1995; Kabanov et al. 1997b; etc.). The data obtained were also used to validate the results of satellite observations (Ignatov et al. 1995). In our experiments we used the sun photometer in the wavelength range from 0.37 to 1.06 μm (part of the data was derived in the range of up to 4 μm). In addition to AOD, the atmospheric columnar water vapor W was measured using the differential technique in the absorption band 0.94 μm. In the present paper we generalize our previous results related to the spatial distribution of transparency and the features of spectral behavior $\tau^A(\lambda)$ over different areas of the ocean.

2. Experiment and methodology

a. General characteristics of the experiments

Measurements of the atmospheric transparency carried out in five expeditions cover the greater part of the central and North Atlantic (latitudinal zone from 10°S to 60°N), as well as the North and the Mediterranean Seas. Experimental sites and the routes of the research vessels (Fig. 1) give a general idea of the operational locations. Particular significance was attached to the continuity of the observation series in the course of each day and the total period of measurement. Table 1 shows that the total array of measurements amounted to 264 days and the degree of regularity of observations (except for 1989) was maintained at the level of 0.9. Hourly observations were performed in 10–50-min-long series, provided there were favorable atmospheric conditions (cloudiness, precipitation, etc.). Preliminary data analysis was limited to individual geographical regions without accounting for the peculiarities of the spatial distribution of aerosol over the ocean. In the course of revealing the pattern of the spatial distribution τ^A_λ we formulated the principles of transparency zoning on the basis of earlier investigations (Kondratyev et al. 1983; Barteneva et al. 1991; Volgin et al. 1988; etc.), and further analysis was carried out for separate ''aerosol'' regions with similar characteristics. Depending on the problem at hand, two types of data were used for interpretation: the hourly mean and the daily mean values τ^A_λ.

TABLE 1. Information about oceanic expeditions (N is the duration of measurements, n is the number of the days of measurement, n/N is the observation regularity degree, and k is the number of hourly mean readings).

Number of cruise–ship's name	Period	N	n	n/N	k
40–*Academik Vernadsky,* Russia	Aug–Dec 1989	111	68	0.61	252
43–*Academik Vernadsky,* Russia	Jul–Oct 1991	91	83	0.91	450
Esperanza del Mar, Spain	Apr–May 1994	21	19	0.90	156
35–*Academik Mstislav Keldysh,* Russia	Jan–Apr 1995	83	73	0.88	496
39–*Academik Mstislav Keldysh,* Russia	Aug–Sep 1996	26	25	0.96	169

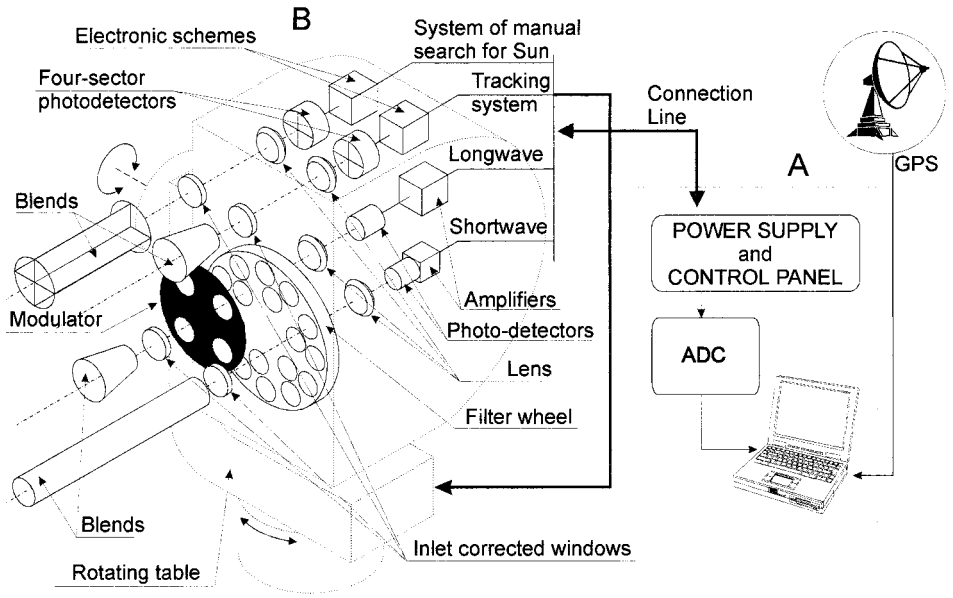

FIG. 2. Scheme of sun photometer SP-3.

b. Instrumentation

The first measurements (1989) used a simple photometer described by Korotaev et al. (1993). Later, a few modifications of the multiwave automated sun photometers specially designed for marine researches were introduced at the Institute of Atmospheric Optics (Kabanov et al. 1993; Sakerin et al. 1996). Let us briefly describe the base variant of the device (Fig. 2).

Shipborne conditions of operation dictated the implementation of sun photometers in two separate parts: the control and recording system (A) stationed in the laboratory, and the remote optical and electronic unit (B) on a two-coordinate rotating table that can be placed on the upper deck at the distance of up to 20 m away. To reduce the influence of external factors (humidity, temperature, electromagnetic stray signals), the optical and electronic unit is put in a shielded thermostatic moisture-proof case. The photometer includes the automated sun tracking system, shortwave (0.37–1.06 μm) and longwave (2–4 μm) measurement channels. The main parts of the shortwave channel are a color-correcting inlet window (for spectral equalization of the signals), a quartz lens, and the photodetector. The hybrid integral photodetector includes a silicon photodiode and an amplifier with a switchable amplification coefficient. The longwave [infrared (IR)] measurement channel consists of an inlet window, a germanium lens, and a pyroelectric detector with a selective amplifier. The wavelength tuning is performed by a continuously rotating barrel with interference filters and a synchronization scheme that produces the service signals. The specifications of the photometer is given in Table 2.

The sun tracking system consists of a four-sector photodetector placed at the lens' focus, and the electronic scheme that drives the rotating table. The recording system includes the control unit, the analog–digital converter and a personal computer. Measured and service signals are fed into the computer during the operation. Exact time and navigation data from the global positioning system are input through the serial port.

The measuring and data processing program performs the following basic operations: (a) sorts out the signals by spectral channels with reference to the time and coordinate readings; (b) accumulates and filters the signals and calculates the optical air mass; (c) performs intermediate calculation of τ_λ^A and W, which, in real time,

TABLE 2. Main characteristics of the multiwave sun photometer (1995 version).

Characteristics	Shortwave channel	Longwave channel
Field-of-view angle (°)	0.75	1
No. of spectral channels	12	6
Maxima (half-widths) of the band-pass filters (nm)	368 (22); 408 (30); 423 (13); 438 (6); 484 (7); 513 (20); 553 (8); 637 (5); 673 (10); 871 (11); 940 (10); 1061 (19)	2181 (22); 2317 (27); 2065 (27); 3906 (50); 3998 (57); 0.35÷3.5
Error of measurements (%)	0.3	0.7
Time of single measurement(s)	40–60	
Error of solar tracker (°)	0.2	

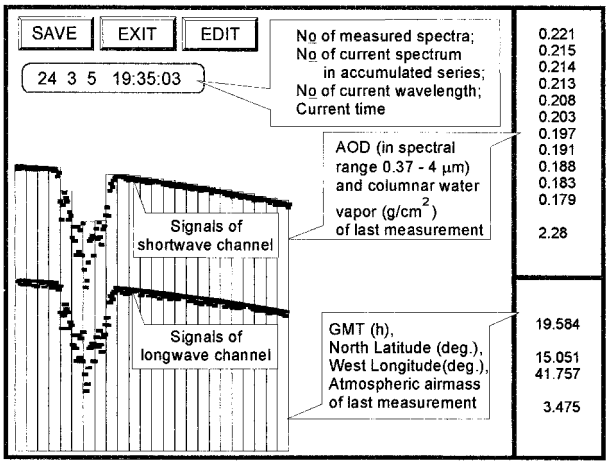

FIG. 3. Data display during experiment (short time decrease of the signals is related to a semitransparent cloud).

are displayed on the screen in graphic and numerical form (Fig. 3); (d) an operator monitors the process of measurement, makes decisions, and stores the accumulated data in memory; (e) if necessary, the operator edits the readings, that is, removes the false readings displayed on the screen as a result of cloudiness or of the ship's structures caught in the field of vision.

c. Methodology

The atmospheric sun photometry is based on the Bouguer–Lambert law that relates the measured direct solar radiation to the atmospheric transparency T_λ^Σ (e.g., Shaw et al. 1973; Gushin 1988):

$$U_\lambda = \rho U_{0\lambda} T_\lambda^\Sigma = \rho U_{0\lambda} T_\lambda^W T_\lambda^X T_\lambda^C \exp[-M(\tau^R + \tau^A)], \quad (1)$$

where $M(Z)$ is the atmospheric air mass at the solar zenith angle Z, ρ is the correction term to Earth–Sun distance, U_λ is the measured signal of the solar spectral radiation, $U_{0\lambda}$ is the extraterrestrial (calibrating) signal, τ_λ^R is the spectral optical depth of Rayleigh scattering, $\tau_\lambda^W(\tau_\lambda^X, \tau_\lambda^C)$ is the spectral optical depth of H_2O (O_3, constant gases) absorption.

The traditional technique used to determine the value of τ_λ^A is based on the assumption that the absorption is small and the logarithm of the measured transparency signal depends linearly on the optical air mass. In this case the linear extrapolation of the signals, $\ln[U_\lambda(M)]$, to $M = 0$ determines the unknown value, $U_{0\lambda}$, [Langley-plot slope method (e.g., Ångström 1961; Forgan 1994)]. After the calibration, Eq. (1) yields the value of τ_λ^A:

$$\tau_\lambda^A = M^{-1} \ln[U_{0\lambda}(\rho/U_\lambda)] - (\tau_\lambda^R + \tau_\lambda^W + \tau_\lambda^X + \tau_\lambda^C). \quad (2)$$

At the first stage of our investigation, in order to find τ_λ^A in the spectral range to 1 μm, we employed an analogous technique (Korotaev et al. 1993). A small contribution that comes from the optical depth of gases was excluded using the LOWTRAN-6 code (Kneizys et al. 1983).

In the IR "transparency windows," even when working with a high spectral resolution, it is practically impossible to single out the bands that are completely free of absorption. It indicates that a more thorough calculation of absorption is required, which would account for the change of concentration of "variable" gases (H_2O, O_3) and overcome the calibration difficulties due to the nonlinear dependence of $\ln(U_\lambda)$ and $\ln(T_\lambda^\Sigma)$ on the air mass M. In addition, at large zenith angles the air mass of separate atmospheric components (aerosol, ozone, etc.) starts to differ due to the difference in vertical density distribution (e.g., Kasten 1966; Reagan et al. 1986). So another technique for calculation of τ_λ^A was developed for the extended spectral range. The main principles applied to determine the τ_λ^A in the shortwave range were considered by Ignatov et al. (1994) and the final formulation of the calculation procedures were presented by (Kabanov et al. 1997a). Spinhirne et al. (Spinhirne et al. 1985; Shiobara et al. 1996) were first to use an analogous approach, but there are some differences. The principal idea is to apply the absorption exclusion directly to the original data, that is, the signals U_λ. In the traditional technique the absorption is taken into account at the final stage; after the calibration and when the total optical depth is evaluated. Below we briefly describe the algorithm to determine the τ_λ^A.

The gases' transmission functions are calculated with the use of the LOWTRAN-7 code (Kneizys et al. 1988) where we take into account the solar radiation spectra and the transmission of filters and inlet windows (the spectral instrumental function, A_λ):

$$T_{\Delta\lambda}^j = \left(\int_\lambda A_\lambda T_\lambda^W T_\lambda^X T_\lambda^R \, d\lambda \Big/ \int_\lambda A_\lambda \, d\lambda \right), \quad (3)$$

where $T_{\Delta\lambda}^J$ is the integral transmission function of jth spectral channel.

The necessity to use Eq. (3) in calculations was dictated not only by the finite character of the photometer spectral resolution but also by the significant effect of the "wings" of the spectral transmission of the interference filters. The estimation showed that the negligence of the latter factor especially affects the spectral channels near the absorption bands.

To calculate the transmission function T_λ^R, we used the expression that takes into account the deviation of the atmospheric pressure p from the standard pressure p_0 (Hansen et al. 1974):

$$T_\lambda^R(M) = \exp\{-M[0.008569\lambda^{-4} \times (1 + 0.0113\lambda^{-2} + 0.00013\lambda^{-4})]p/p_0\}. \quad (4)$$

The transmission functions of the "constant" gases (CO_2, CH_4, N_2O, CO, etc.), as a result of small spatial and temporal variability, were determined within the framework of the five standard models of LOWTRAN-

7, and the results of the calculation were approximated by the exponential dependencies of the form

$$T_\lambda^C(M) = \exp(-aM^b), \quad (5)$$

where a and b are the approximation parameters obtained by the least squares method.

Approximations for T_λ^X were selected in an analogous way, except for the ozone concentration X where we used the more detailed data of the 2D model (latitude and month; Tanre et al. 1992).

The function T_λ^W brings about maximum distortion in the IR transparency windows and is most subject to variations. Obviously, it is more efficient to take into account the real variations of W by the differential technique (e.g., Reagan et al. 1992) using the result of simultaneous measurements of the water vapor absorption in the 0.94-μm band. In this case it is expedient to exclude intermediate calculations of W and determine T_λ^W directly as a dependence on the ratio of the signals measured in the range of the H_2O absorption band. The formula was chosen by the least squares method for calculation of T_λ^W in the form of the exponential decay function (Kabanov et al. 1997a)

$$T_\lambda^W = \zeta + \sum_{\kappa=1}^{2} \mu_\kappa \exp\{[\eta - U_{0.94}(U_{0.87}V_0)^{-1}]\nu_\kappa\}, \quad (6)$$

where $(U_{0.94}/U_{0.87}) = T_{0.94}^W V_0$ is the signal ratio proportional to the water vapor absorption in the range of 0.94 μm; and V_0 is the calibration constant determined by the modified Langley approach (e.g., Reagan et al. 1992); ζ, μ, η, and ν are the approximation parameters. Note that the dependence of T_λ^W on the air mass M does not explicitly appear in Eq. (6) because it is already embedded in the ratio $(U_{0.94}/U_{0.87})$.

After the calculation of T_λ^i and then $T_{\Delta\lambda}^j$ for each spectral channel, one can get the aerosol signals Y_λ^J, which are free of absorption:

$$Y_\lambda^j(M) = U_\lambda/T_{\Delta\lambda}^J = U_{0\lambda} \exp(-\tau_\lambda^A M). \quad (7)$$

The logarithms of the aerosol signals Y_λ^j depend linearly on the air mass M, so there is no doubt about the correctness of the calibration. After the calculation of $U_{0\lambda}$, the standard Langley-plot method yields the value of τ_λ^A in the form

$$\tau_\lambda^A = M^{-1} \ln(U_{0\lambda}/Y_\lambda^J). \quad (8)$$

Note that the transmission functions of separate atmospheric components along with their air masses M_i are calculated independently [Eqs. (4)–(7)]. Therefore, the technique considered makes it possible to relatively simply extend the measurements to zenith angles of about 85° and take into account the individual dependencies $M_i(Z)$ (Sakerin et al. 1997). Thus, there is no need to do more complex iteration calculations (e.g., Forgan 1988).

d. The calibration and accuracy of the retrieved τ_λ^A

The accuracy of the calibration affects the quality of experimental data to a significant degree. A majority of the investigators were engaged in the development and improvement of new calibration techniques (e.g., Herman et al. 1981; Soufflet et al. 1992; Forgan 1994). To reach a higher calibration accuracy, it is necessary to select days with a stable atmosphere, high transparency, and a wide range of the air mass M. The calibration of 1989 measurements was based on the Langley plot procedure. Later an iteration algorithm for the calculation of $U_{0\lambda}$ was developed by our coauthors (Ignatov et al. 1993). It is based on the assumption that the variations of AOD under conditions of high transparency are insignificant and practically do not depend on the air mass. In other words, at minimum values of τ^A its variations are of the same order of magnitude as the measurement error. In this case, the sought, U_0^*, and the true, U_0, values of the calibration constant can be related via the expression $U_0^* = U_0(1 + k)$, and one can select the U_0^* using the regression equation

$$\tau^* = \upsilon + (\varepsilon \pm \delta_\varepsilon)M^{-1}, \quad (9)$$

where ε and δ_ε are the systematic and random errors of U_0 selection.

The quality of the selection of U_0^* is determined by the operator in the dialog mode from the shape of the displayed dependence $\varepsilon(\tau_i^*)$, where τ_i^*, is the variable upper boundary of the subarray of optical depths ($\tau^* < \tau_i^*$), on which the parameter ε is calculated. The selection criterion is the convergence of the values $\varepsilon(\tau_i^*)$ to zero as τ_i^* decreases. To exclude the subjective character of the dialog selection and reduce the calibration procedure of the multiwave data, an algorithm was developed based on the formalized criterion for the selection of U_0^*. The following values are used for calculation:

$$\Theta = \sum_{j=1}^{10} |\varepsilon(\tau_j^*)| \quad \text{and} \quad \delta_\Theta = \sqrt{\sum_{j=1}^{10} \delta_\varepsilon^2(\tau_j^*)}, \quad (10)$$

where ε is calculated on the subarray $\tau_{\min}^* \le \tau^* \le \tau_j^*$, and $\tau_j^* = \tau_{\min}^* + 0{,}005\,j$. The parameter ε is calculated only if the number of experimental points falling into the subset is greater than five. The character of the dependencies $\Theta(U_0^*)$ and $\delta_\Theta(U_0^*)$ shows that the convergence of the values of U_0^* and U_0 is accompanied by a decrease of the values of Θ and δ_Θ (Fig. 4). The most exact selection of U_0^* corresponds to the minimum of Θ and δ_Θ. The accuracy of the algorithm was checked by comparing the results of calibration with other methods: (a) the dialog variant (Ignatov et al. 1993); and (b) the standard Langley plot technique applied to the results of measurements in mountains (Tenerife Astrophysical Observatory, Mt. Teide, 2.38 km). From the derived data it follows (Table 3, Fig. 5) that the difference in the results of different methods does not exceed $\pm 0.3\%$. The results of one more comparison of cali-

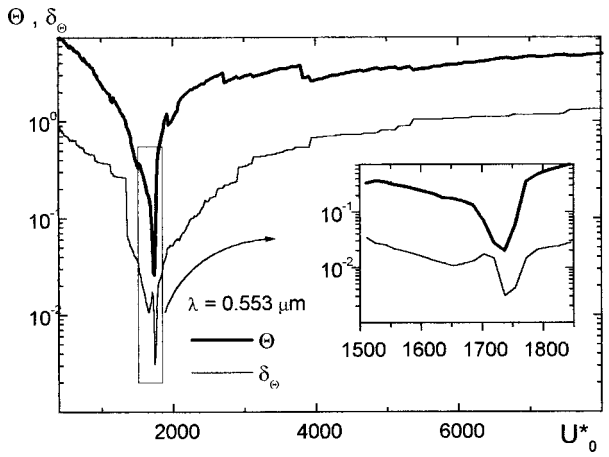

FIG. 4. Illustration of the dependencies of $\Theta(U_0^*)$ and $\delta_\Theta(U_0^*)$ used to determine U_0.

brations (for 1996) are plotted in Fig. 6. Here we give the relative differences between the calibration signals $\Delta_i = (U_{00} - U_{0i})/U_{00}$ calculated for the following versions: 0) iteration algorithm applied to the entire data array, 1) iteration algorithm applied to before-noon measurements, 2) iteration algorithm applied to afternoon measurements, 3) iteration algorithm for the first half of the cruise, 4) iteration algorithm for the second half of the cruise, and 5) standard Langley plot method. The calculations showed that the mean deviation from the basic version (U_{00}) is $\pm 0.5\%$ in the entire spectral range. Comparing versions 3 and 4, we can conclude that the photometer is stable enough. Similar estimates for the earlier period were given in Ignatov et al. (1993).

Thus, the iteration algorithm (10) substantially simplifies the calculation procedure for qualitative data $U_{0\lambda}$. The essential requirement here is the accumulation of a sufficiently long series of observations, including measurements made during high atmospheric transparency. For this reason, the main difficulty we encountered during our cruises was in providing long-term stability of the photometer operation under the complex influence of the environment (ship rolling, vibration, wave spray). In two cruises (1991 and 1995) we had to perform recalibration because of equipment failure. To reduce the risk of a short ''uncalibrated'' array of data, in the last expedition we used the reference lamp source of stable radiation.

The accuracy of determination of τ_λ^A was earlier analyzed in detail by Kabanov et al. (1997a). Here we give a brief summary of the results. The calculations for concrete experimental conditions showed that random errors of the signal measurement and determination of the optical air mass are minimum. The major contribution comes from systematic error due to the calibration and the presence of gas components. Applying the ''aerosol signals'' technique, the total error to determine τ_λ^A was estimated by the value of up to 0.01 in the visible range and 0.01–0.015 in the range of 2–4 μm. It should

TABLE 3. Comparison of $U_{o\lambda}$ calculated by different methods (example of the results of 1994).

λ, μm	0.369	0.408	0.423	0.438	0.484	0.514	0.553	0.637	0.673	0.871	1.061
Langley plot (Mt. Teide)	1659	2232	2460	2294	2468	2182	1734	942	1733	1410	799
Dialogue algorithm (9)	1650	2229	2450	2285	2482	2190	1730	—	—	—	—
Iteration algorithm (10)	1659	2223	2456	2286	2480	2186	1733	942	1731	1405	797
Difference of $U_{0\lambda}$, ± %	0.27	0.20	0.20	0.20	0.28	0.18	0.12	0	0.06	0.17	0.25

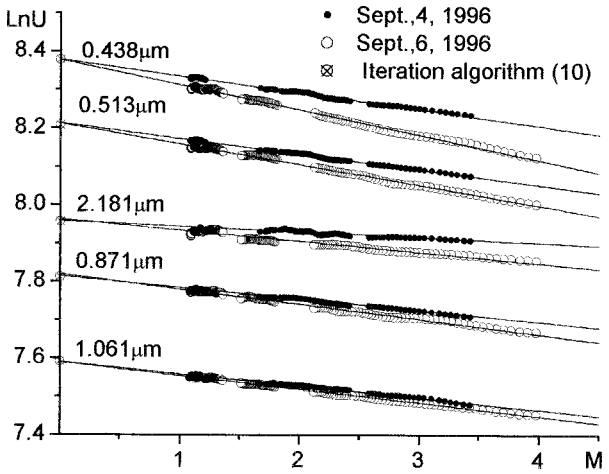

FIG. 5. Example Langley plots for several wavelengths (1996).

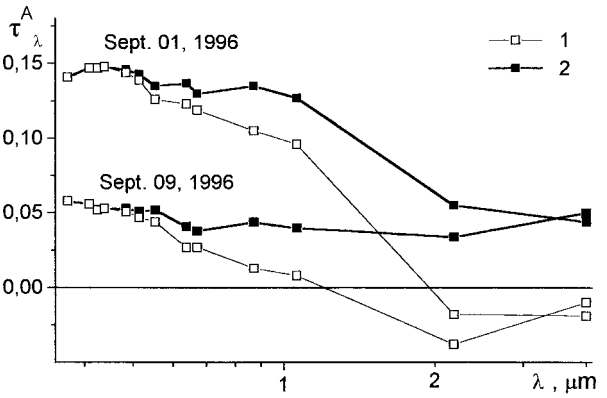

FIG. 7. Difference in the determination of τ_λ^A: 1 is the traditional method; 2 is the aerosol signal method.

be emphasized that such accuracy in the IR range is possible if one takes into account the ''nonlinear'' effect of gas absorption and the real variability of water vapor in the atmosphere. Neglecting these factors increases the error by several times. For example, if one uses the traditional technique and the modeled values of W, the error estimate for the spectral channel 2.18 μm will amount to $\sim$0.07. The alternative calculations of τ_λ^A (Fig. 7) give a clear example of the inapplicability of the traditional technique [see Eq. (2)] in the IR range. The difference in the results obtained by the two techniques in the visible range is insignificant. Systematic underestimation of the values of τ_λ^A is observed in the IR range, which additionally increases because of the big difference between the actual concentration of the atmospheric water vapor ($\sim$1.4 g cm^{-2}) and the modeled one ($\sim$2.356 g cm^{-2}).

3. Results and discussion

Geographic distribution of AOD over the ocean is diverse and covers almost two orders of magnitude (Barteneva et al. 1991; Volgin et al. 1988; Smirnov et al. 1995b; etc.). The variations observed pertain not only to the value of aerosol turbidity but also to the character of its variability and the spectral behavior of $\tau^A(\lambda)$. The wide scatter from 0.05 to 0.5 and more is observed even in the mean values obtained by different authors. One might have doubts about the representativity of individual results, but the principal reason for the differences is objective. It is difficult to expect the same characteristics of atmospheric turbidity over a large territory of the ocean, bordering on both pure polar areas and the continents that generate different types of aerosols. The results shown in Fig. 8 illustrate the range of variability of AOD and the Ångström parameter α, which characterizes the selectivity of the spectral behavior (e.g., Ångström 1961; Shaw et al. 1973).

$$\tau^A(\lambda) = \beta\lambda^{-\alpha}, \tag{11}$$

where $\beta \approx \tau^A$ (1 μm) is the atmospheric turbidity coefficient depending on the aerosol density.

There are possible differences when comparing with the results of other authors because of different tech-

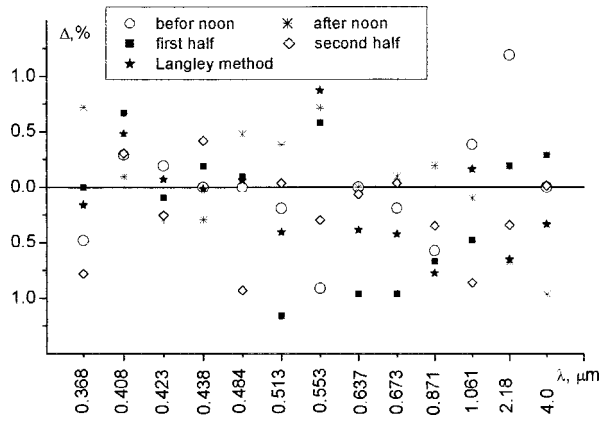

FIG. 6. Relative differences of calibration constants for different wavelengths.

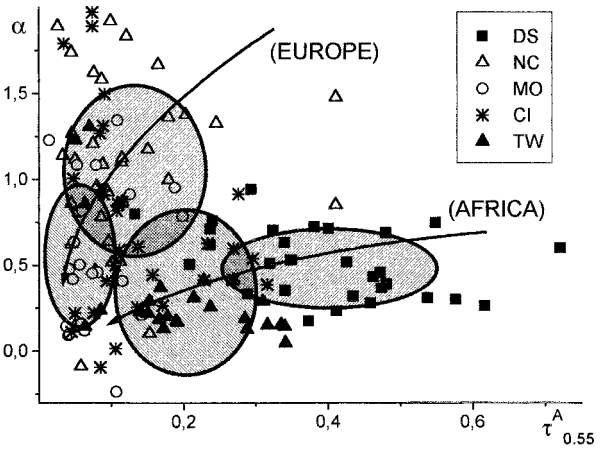

FIG. 8. Correlation between $\tau_{0.55}^A$ and α (location of the characteristics of the principal regions are circled).

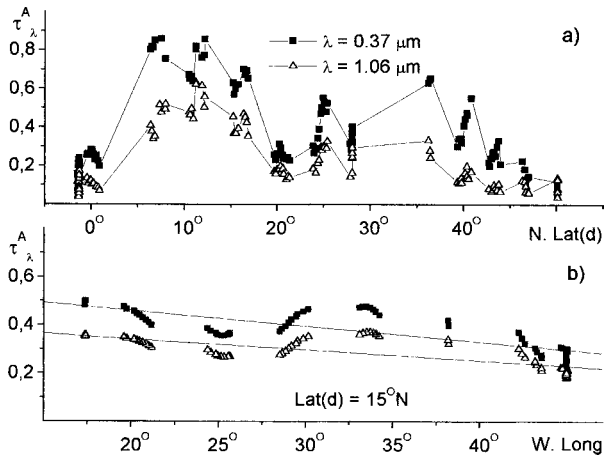

FIG. 9. Examples of (a) latitudinal and (b) meridional dependencies of τ_λ^A.

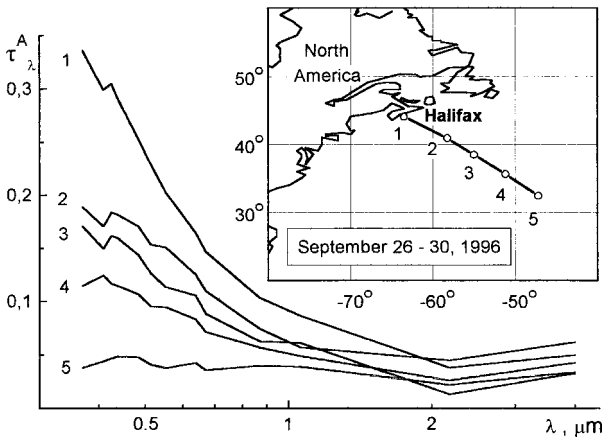

FIG. 10. Transformation of the spectral behavior of $\tau^A(\lambda)$ at temperate latitudes when moving out of the continent.

niques applied to calculate α and β (Cachorro et al. 1987; Cuomo et al. 1993; etc.) We used hourly mean and daily mean spectra of τ_λ^A in the range from 0.37 to 1.06 μm. The parameters α and β were calculated by the least squares method after taking logarithm of the dependence Eq. (11).

The spatial variability of τ_λ^A at the change of latitude and the distance from the continent is shown in Figs. 9 and 10. On the whole, the total range of variability of $\tau_{0.55}^A$ over the Atlantic Ocean lies within a range from 0.01 to 0.7 and the Ångström parameter varies from -0.24 to 2.42. Given this wide scatter of the values of τ_λ^A, the necessity of zoning becomes obvious.

a. Genetic zoning

In the existing climatic zoning methods one can single out two classification groups: genetic and ''sign'' (Samoilenko 1983). Obviously, aerosol as an element of a climatic system can be subjected to analogous classification. For the oceanic areas, genetic zoning appears preferable since it reveals the main processes forming the atmospheric physical fields and enables us, in the case of insufficient data, to extend the revealed features to less studied areas. The atmospheric circulation and peculiarities of the underlying surface play an important role in many genetic classifications (Alisov et al. 1974; Flohn 1957; Samoilenko 1983; etc.). The type of underlying surface also determines the majority of aerosol sources and the aerosol spatial distribution depends on the air masses transport. The following feature is essential for the atmosphere over the ocean.

Microphysical and optical investigations of aerosol over the ocean (e.g., Kondratyev et al. 1983; Reddy et al. 1990; Barteneva et al. 1991; Smirnov et al. 1995a) showed that in spite of the homogeneity of the underlying surface (the generator of marine aerosol) and the smooth variation character of meteorological fields, the variations of the aerosol characteristics are significant and in many respects are influenced by the intrusion of different types of continental aerosol. One can draw an obvious conclusion from this fact that the transfer of continental aerosol leads to spatial inhomogeneities of AOD over the ocean. Thus, the classification of the aerosol fields should take into account the combined effect of two principal factors: the sources (types) of aerosol prevalent in each latitudinal zone and the prevalent circulation of air mass that determines the depth and the direction of aerosol emission into the oceanic atmosphere. For this reason, we did not use our optical data for the genetic zoning, instead we leaned upon the results of investigation of the wind characteristics (Roll 1965; Kool 1975) and the aerosol composition in different areas (Prospero 1979; Kondratyev et al. 1983; Hoppel et al. 1990; Fitzgerald 1991; Barteneva et al. 1991; etc.). The atmosphere over the major space of the ocean is characterized by the variety of circulation, climatic conditions and aerosol sources. Nevertheless, it is sufficient to select three principal zones (temperate, tropical, and equatorial) in the latitudinal division (except the Arctic), which simultaneously take into account both the difference in aerosol sources and transfers.

In the temperate latitudes a finer aerosol prevails over the sea-originated aerosol (e.g., Barteneva et al. 1991). A narrow littoral zone (LZ) can be marked out along the continental border where the breeze circulation mixes up the continental and sea aerosols, and thus enriching the latter with the fine fraction. The extension of this area from the coast can be estimated by tens of kilometers. The developed cyclonic activity typical of these latitudes and the westward transfer provide subsequent migration of continental aerosol into the ocean. Moving farther into the ocean, the air mass loses continental aerosol while the concentration of sea aerosol increases. So one should separate the near-to-continent (NC) areas and the most remote midocean (MO) areas.

Our optical data (Fig. 10) confirms the redistribution of fine and coarse aerosols as one moves farther from

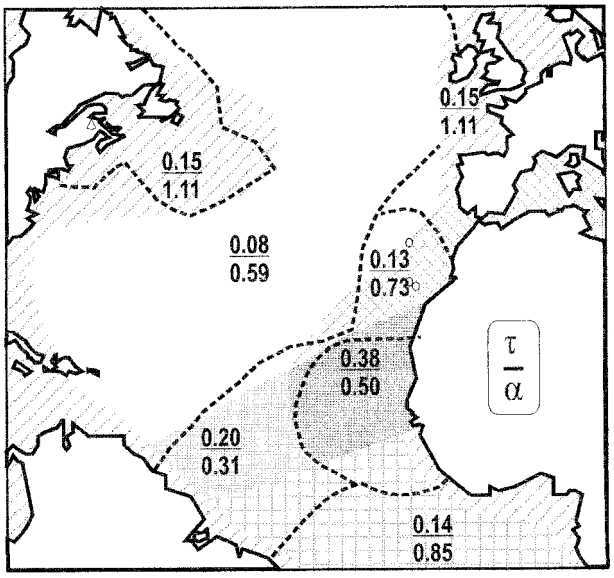

FIG. 11. Location of the ''aerosol areas'' as result of the genetic and ''sign'' (dotted line) classification.

the continent. A large concentration of fine aerosol in the coastal zone determines the high selectivity of the spectral dependence of $\tau^A(\lambda)$. As the distance from the coast increases, the spectral behavior becomes more flat because of τ^A_λ decrease in the shortwave range. The shortage of data and the random character of transfer prevents an exact separation of NC and MO areas. For this reason, we will make use of a semiqualitative estimate based on the scale of cyclonic formations. Accounting for the different intensity of aerosol sources and transfers at different latitudes, the extension of NC can be estimated as 100–200 km at the boundaries of the temperate latitude zone and up to ~1000 km in its middle part (Fig. 11).

At tropical latitudes the stable trade wind transfer accompanied by the emission of coarse dust aerosol from the Sahara Desert is predominant. It is well known from the coast-based, shipborne and spaceborne investigations (e.g., Prospero 1979; Hoppel et al. 1990; Barteneva et al. 1991; Swap et al. 1996) that the content of the Sahara aerosol gradually decreases, but still can be traced up to the coast of America. The inversions and relatively high transfer speed in the layer from 2 to 4 km, which is characteristic of the trade wind zone (TW), favor this fact. One can assume based on the aerosol characteristics that the TW reaches the west coastal areas of the Atlantic. Correspondingly, the MO area narrows in the southward direction and is restricted to the TW. The TW area, most rich in dust aerosol (eastward of 35°W), is known in literature as the ''Dark Sea'' (DS). The natural southern boundary of DS and TW lies in the intertropical convergence zone (IC), for which the annual mean position is near 7°N (e.g., Kool 1975]. The IC axis, as well as the trade wind axis, are deflected from east-northeast to west-southwest.

The mixed areas, the Canary Islands (CI) and the Mediterranean Sea (MS), should be marked out in the northeast of the tropical zone. These areas, depending on the seasonal circulation, are alternatively affected by the emission of fine and coarse aerosols from Africa and Europe. The change of circulation is caused here by the proximity of the northeast trade wind to the Azores anticyclone—one of the main centers of atmospheric activity.

At last, in the southern part of our investigation area there is located the equatorial zone or IC. This zone has the following typical geophysical conditions: calm wind, developed convection, filtration of continental aerosol by cloudiness, and frequent precipitation (e.g., Samoilenko 1983; Barteneva et al. 1991). All these conditions form a character of aerosol turbidity different from the neighboring trade wind zone.

b. Sign zoning

To confirm the results of genetic zoning, we further applied the sign classification. In the sign classification, the zones are chosen based on several directly measurable quantitative characteristics of the atmosphere (Samoilenko 1983). Pertaining to AOD (Volgin et al. 1988) it was shown that in order to reveal optical differences in the atmosphere over different areas, it is sufficient to consider two signs: the value of $\tau^A_{0.55}$ and the Ångström parameter α.

The zoning procedure included two stages. First, the isolines of the characteristics were drawn on the map (Fig. 12). The values of $\tau^A_{0.55}$ and α were averaged over the squares with the step of 5° in latitude and longitude, and the missing points were added from interpolation and extrapolation of the data. The obtained results agree with genetic zoning. For example, the distribution of isolines at temperate latitudes confirms the increase of $\tau^A_{0.55}$ and the selectivity of the spectral behavior α when approaching the continents both from westward and eastward directions. The trade wind zone reveals a different pattern. The value of turbidity continuously increases from America to Africa, and the parameter α has minimum in the middle part of the ocean with a concentric distribution of isolines (an increase in all directions).

At the second stage we determined the zone boundaries. The selection criterion for the MO zone was the fall of $\tau^A_{0.55}$ and α obtained at the central part of temperate latitudes, into the interval ''mean plus standard deviation.'' The separation of the MO and NC areas was actually determined by the boundaries of the values of $\tau^A_{0.55}$. The boundary selection criteria in the tropical and equatorial zones were the qualitative differences in the character of the spatial distribution of $\tau^A_{0.55}$ and α. The boundaries were drawn in the places of minimum gradients or minimum values of the parameters between the neighboring areas. As a result, the revealed ''aerosol

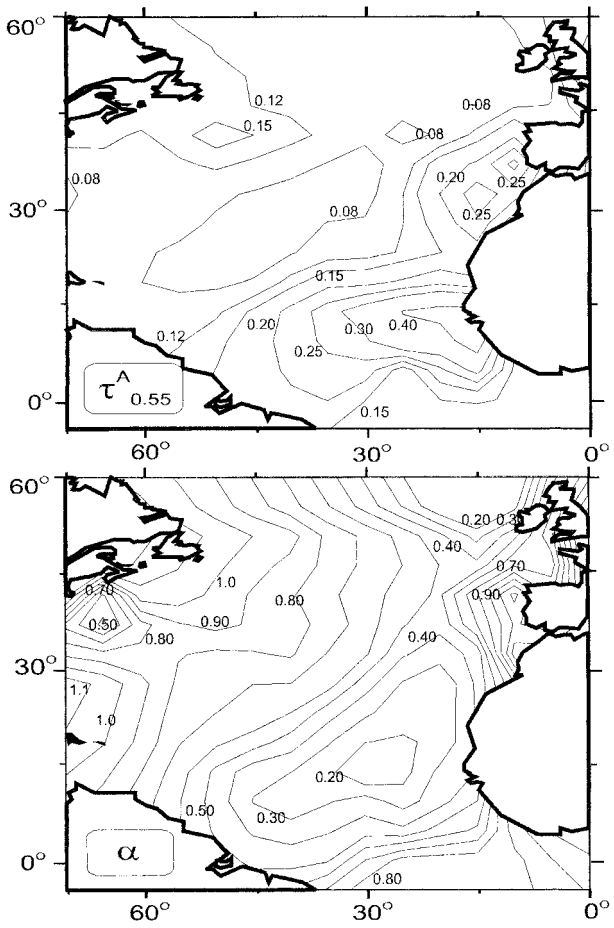

FIG. 12. Isolines of the spatial distribution of $\tau^A_{0.55}$ and α.

provinces'' came out close enough to the genetic zoning data (Fig. 11).

The quantitative characteristics of AOD for the separated areas of the ocean are presented in Table 4. For different areas the samples obtained statistically differ in at least one parameter with the confidence interval of no less than 0.9. Calculating the characteristics of $\tau^A_{0.55}$, we did not perform the averaging of our data with the data derived by other authors for the reasons of methodic character: different ways of accounting for the gas components (some papers do not exclude the absorption at all), differences in statistical provision and averaging techniques, etc. For the LZ, due to insufficiency of our data taken near the coastal areas, we give the data from the paper (Volgin et al. 1988).

Table 4 gives a good picture of the differences between the aerosol provinces with regard to the mean values of AOD, parameter α, and the variation coefficients V_τ. The enhanced turbidity near the continents (NC, DS, CI) is obvious. Also there is no need to comment on the fact that the Ångström parameter grows when approaching Europe (America) from the oceanic values 0.6 and approaches the continental values [$\alpha \approx$ 1.3–1.6 (e.g., Barteneva et al. 1991; Halthore et al. 1992; Cachorro et al. 2000)]. Approaching Africa, the turbidity increases due to the enrichment by coarse dust particles. So the variations of the parameter α are less significant. The areas with the developed cyclonic activity (MO, NC, CI, and MS) are characterized by the maximum relative variability of the value of τ^A_λ. The variation coefficients V_τ are over 60% here and exceed analogous characteristics of the continental atmosphere (Kabanov et al. 1996). Let us make two notes pertaining to the considered characteristics.

1) Our calculations of statistical characteristics (Table 4) did not use the measurements taken in 1991, 1–3 months after the Mt. Pinatubo eruption (Sakerin et al. 1993; Zyev et al. 1997). The characteristics of τ^A_λ obtained during this period in the CI, MO, and NC areas are in agreement with the applied classification, though the values of τ^A_λ and α are distorted by additional contributions from the volcanic layer.
2) The results obtained in the MS zone are not sufficiently representative because of scanty measurements made in this area. The values of τ^A_λ are noticeably lower as compared to more representative data by (Shifrin et al. 1980; Volgin et al. 1988; Smirnov et al. 1995b). Due to the circulation peculiarities of this region, either clear-air masses from the ocean or the continental emissions from Europe and the Sahara are prevailing in this area in different seasons and synoptic periods. As it follows from the results obtained, in our case it was mostly the oceanic air.

c. Statement and comparison of the results

A good confirmation of the reliability of the performed zoning is the agreement between the results of

TABLE 4. Mean values and variation coefficients V of $\tau^A_{0.55}$, and parameters α and β(V = mean/std dev; k is the number of hourly mean readings).

Area	MO	NC	LT*	CI	MS	DS	TW	IC
N (days)	26	25	—	31	6	32	23	25
k	152	120	—	231	41	179	161	155
$\bar{\tau}$	0.076	0.149	0.20	0.135	0.072	0.381	0.196	0.141
V_τ	0.62	0.65	0.49	0.60	0.66	0.38	0.49	0.52
$\bar{\alpha}$	0.59	1.11	0.90	0.73	1.0	0.50	0.31	0.85
V_α	0.80	0.45	—	0.74	0.60	0.45	1.11	0.65
$\bar{\beta}$	0.06	0.08	—	0.09	0.05	0.29	0.17	0.09
V_β	0.61	0.72	—	0.77	1.04	0.46	0.52	0.49

* The results of Volgin et al. (1988).

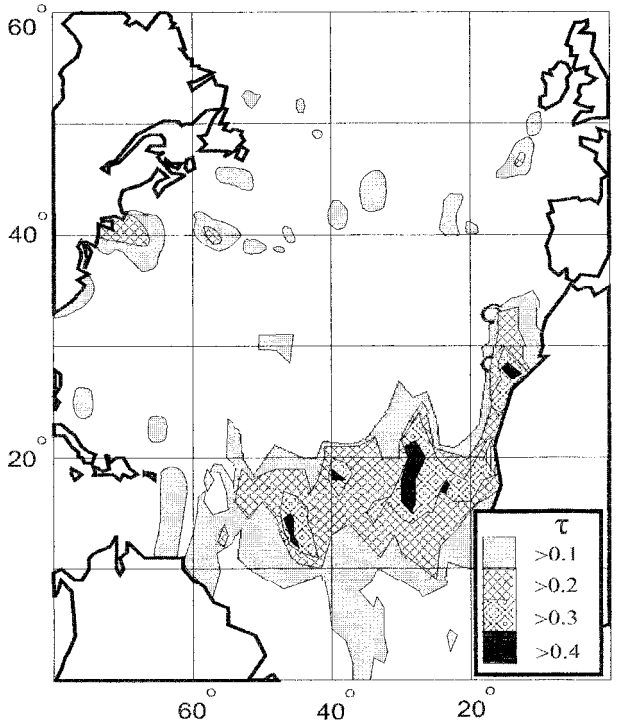

FIG. 13. Spatial distribution of AOD of the atmosphere obtained from the satellite data.

genetic and sign classifications. The ranges of values of $\tau^A_{0.55}$ and α (Fig. 8) are localized in accordance with regional features. The area overlapping and the point scatter are natural due to the synoptic variability of AOD (the intrusion of various air masses into the observation regions). The zoning is in agreement with the spaceborne observation data of AOD over the ocean (e.g., Mishchenko et al. 1999; Swap et al. 1996). As an example, the spatial distribution of τ_{SAT} derived by the AVHRR radiometer during the joint ''satellite–ship'' experiments (Korotaev et al. 1993) is shown in Fig. 13. In spite of the fact that τ_{SAT} data were reconstructed only at one wavelength, the principal peculiarities and the location of the areas correspond to the considered classification.

To estimate the validity of the spatial distribution model of the aerosol turbidity, we will compare our data with the results of other investigations. We will consider mainly the investigations in which the data are most reliable from the viewpoint of statistical and spectral provision (Table 5). The comparison shows that our data fall into the middle range of values published by other authors. Thus, in the MO area the mean values of $\tau^A_{0.55}$ and α are equal to 0.076 and 0.59, respectively, and their whole ranges are limited by the intervals $\overline{\tau}_{MO}$ = 0.067/0.13 and $\overline{\alpha}_{MO}$ = 0.1/84. The exception is the data by (Reddy et al. 1990), and (Ershov et al. 1990; Smirnov et al. 1995b) for 1985 and 1988. In the first case, the value of $\overline{\tau}_{MO}$ = 0.16 is doubtful because the measured values of AOD in the middle of the Atlantic (to the north of 30°N) fell into the range from 0.11 to 0.61 (in fact, they are the same as in a zone of intensive dust emission). However, such a situation cannot be completely excluded for some days. In the second case, the measurements were made to the northwest of Gibraltar where the continental influence of the Pyrenean peninsula and Africa might produce the effect. According to our classification it is the NC area rather than the MO. With this note taken into consideration, our data for the NC area occupy an intermediate position among the whole range of experimental values: $\overline{\tau}_{NC}$ = 0.097/0.23, $\overline{\alpha}_{NC}$ = 0.1/1.65.

The scatter of the mean values in a relatively small DS area $\overline{\tau}_{DS}$ = 0.24/0.54, $\overline{\alpha}_{DS}$ = 0.3/0.6 reflects the seasonal variability and the cyclicality of the dust emissions from the Sahara. Our values of $\overline{\tau}_{DS}$ for different periods of measurements also differ: 0.36 in October 1989, 0.28 in November–December 1989, and 0.48 in April–May 1995, and the total mean value (0.38) is intermediate among all considered results.

Still the question persists: What time period does the obtained characteristics of τ^A_λ correspond to? The scanty and fragmentary character of the investigations over the ocean carried out to date does not allow us to determine the peculiarities of the annual behavior of τ^A_λ. Our measurements were carried out during various, though not all, seasons. When analyzing the results obtained in different months, we have not revealed any differences peculiar to seasonal changes. From general considerations, one can make the following supposition: The marine aerosol is generated round the year, and the effect of the regions with soft climate, where the state of the land remains stable, is prevalent in the emission of continental aerosol. This, of course, does not comprise all possible external effects (the change of circulation, insolation, etc.), but it is enough to suppose that the degree of seasonal variations over the ocean is less than over the land. If one turns to the results of spaceborne observations over the ocean (Mishchenko et al. 1999), then the mean seasonal changes of $\tau^A_{0.55}$ in the Northern Hemisphere can be estimated by the value 0.21 ± 0.02. This value is significantly less than the annual variations of τ^A_λ over the continental areas (Peterson et al. 1981; Gushin 1988; Cachorro 2000) and synoptic variations over the ocean. Thus the characteristics of the spatial distribution of AOD (Table 4) are closer to annual mean estimates.

d. Spectral behavior of τ^A_λ (0.37–1.06 μm)

The spectral behavior of $\tau^A(\lambda)$ in the shortwave range manifests itself in monotonic decrease as the wavelength increases. The empiric Ångström formula [Eq. (11)] is the most widespread form of analytical description for the spectral behavior of AOD (e.g., Ångström 1961; Tomasi et al. 1982; Hoppel et al. 1990; Cuomo et al. 1993). The power dependence of $\tau^A(\lambda)$ is caused by the fact that the submicron aerosol particles, whose relative

TABLE 5. Mean values of $\tau^A_{0.55}$ and α obtained by different authors in three regions.

Areas	Reference	Years	Ocean	N (days)	τ	α
MO	*	1989–96	Atlantic	26	0,076	0,59
MO	Barteneva et al. (1991)	1979	Atlantic	—	0,071	0,1
MO	Barteneva et al. (1991)	1987	Atlantic	—	0,087	0,3
MO	Smirnov et al. (1995b)	1989–90	Atlantic	12	0,07	0,34
MO	Volgin et al. (1988)	1982–86	Pacific**	33	0,07	0,40
MO	Barteneva et al. (1991)	1981	Indian**	15	0,067	0,60
MO	Hoppel et al. (1990)	1983	Atlantic	7	0,13	0,84
MO	Reddy et al. (1990)	1988	Atlantic	6	0,16	1,0
MO–NC	Smirnov et al. (1995b)	1985	East Atlantic	11	0,18	0,56
MO–NC	Yershov et al. (1990)	1988	East Atlantic	15	0,12	0,66
NC	*	1989–96	West and East Atlantic	25	0,149	1,11
NC	Barteneva et al. (1991)	1979	Caribbean Sea	—	0,097	0,1
NC	Hoppel et al. (1990)	1983	Near SE coast of United States	2	0,18	1,65
NC	Barteneva et al. (1991)	1983	Norwegian Sea	—	0,201	0,3
NC	Hoyningen-Huene (1987)	1985	NE Atlantic, North Sea	8	0,23	—
NC	Volgin et al. (1988)	1986	Mediterranean Sea	27	0,20	1,17
NC	Yershov et al. (1990)	1988	Mediterranean Sea	19	0,21	0,86
NC	Wolgin et al. (1991)	1988	Norwegian Sea	9	0,11	—
NC	Villevalde et al. (1994)	1989	Norwegian Sea	7	0,11	0,99
DS	*	1989–95	Tropical Atlantic–dust area	32	0,381	0,50
DS	Volgin et al. (1988)	1986	Tropical Atlantic–dust area	9	0,42	0,45
DS	Barteneva et al. (1991)	1972	Tropical Atlantic–dust area	—	0,24	0,6
DS	Barteneva et al. (1991)	1986–87	Tropical Atlantic–dust area	—	0,535	0,3
DS	Reddy et al. (1990)	1988	Tropical Atlantic–dust area	—	0,37	0,33

* Our data.
** Data obtained in other oceans, presented for comparison.

size ($2\pi r/\lambda$) fall into the beginning of the region of the Mie extinction efficiency factor $Q(r, \lambda) \sim \lambda^{-1}$, usually make the principal contribution into scattering. For coarse aerosol $Q(r, \lambda) \approx 2$, and the spectral behavior is practically neutral. Redistribution of the relative contribution of fine and coarse aerosol particles in the atmospheric column directly affects the spectral dependence of $\tau^A(\lambda)$. One can approximately assume that the parameter β depends on the coarse aerosol density, and α characterizes the concentration of fine particles relative to coarse ones.

The marine atmosphere as compared with the continental one has less concentration of fine aerosol (Kondratyev et al. 1983; Barteneva et al. 1991; Fitzgerald 1991, etc.), so the spectral variations of $\tau^A(\lambda)$ are not very significant. Nevertheless, on average, the monotonic decrease of τ^A_λ is observed in the wavelength range of up to 1 μm. Estimates showed that the mean deviations from the power approximation do not exceed 3%–6% for the majority of areas, and amount to 12% in case of MO. The peculiarities of the variations α have been partially discussed in section 3b. Complete data on the variations of α and β are shown in Table 4. The range of variation of the mean values of α occurs from the minimum values 0.3–0.5 in the trade wind zone to a maximum $\sim$1 at temperate latitudes near the continents (NC, MS). The received allocation of parameter α on the regions is good compared to results of other writers and present representations about the reasons for different selectivity of spectral dependence on AOD (Barteneva et al. 1991; d'Almeida et al. 1991; Volgin et al. 1988; Kondratyev et al. 1983).

There might be some doubts about the fact that the minimum values of $\overline{\alpha}$ occur in a TW area, not in the Dark Sea where the dust concentration is maximum. The matter appears as follows. Indeed, the content of dust aerosol decreases as moving away from Africa due to the spatial spread and fallout of aerosol into the ocean. According to airborne investigations (Kondratyev et al. 1976) during transport, the fine dust particles glue together in conglomerates, which then fall out. That means the dust aerosol size spectrum changes so that the relative concentration of fine particles diminishes. The concentration of other component of the coarse aerosol–salt particles depends on the wind (e.g., Kondratyev et al. 1983; Fitzgerald 1991). Judging from meteorological observations (e.g., Kool 1975), the central part of the Atlantic in the trade wind zone is characterized by the most strong and stable winds. Hence, the generation of marine aerosol here is more intensive than in other areas. The fact that the fallout inversion is weaker here and the upward fluxes become prevalent favors the process of filling the atmosphere of the TW zone with marine aerosol. Thus, the combined effect of the considered factors leads to the increase of the relative content of coarse particles, and the parameter α decreases when passing from DS to TW.

The spatial distribution of the statistical characteristics of β (mean value, standard deviation, max) follows the distribution of the values of AOD with maximum

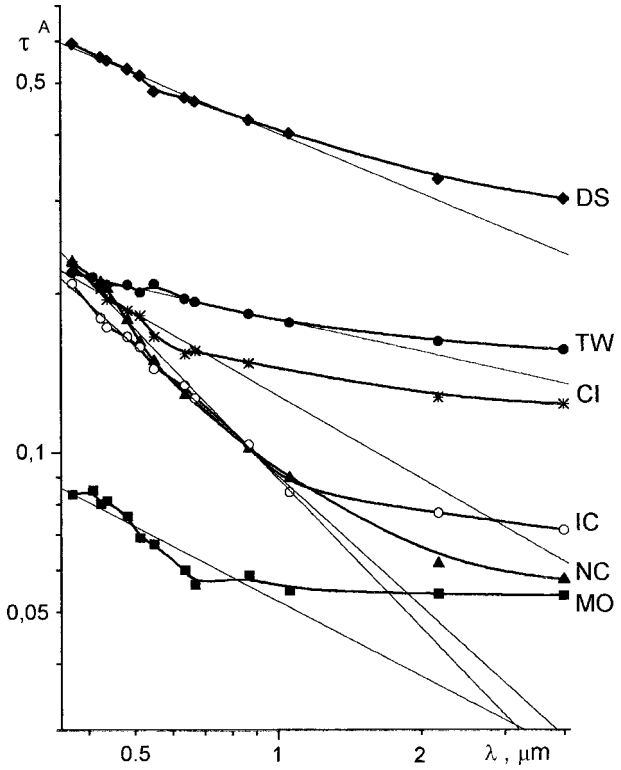

FIG. 14. Mean spectral behavior of τ_λ^A in spectral range 0.37–4 μm [the thin lines is power approximation Eq. (11)].

in the trade wind transfer zone (TW, DS). In the areas far from the dust emission, the mean values of β, as well as of τ_λ^A in IR range (Fig. 14), are approximately equal to 0.05 ± 0.02 and are caused by coarse particles of marine aerosol. One should note a large relative variability of the parameters α and β. High magnitudes of the variation coefficients, ~0.5–1.1, can be explained both as the effect of the airmass change (Smirnov et al. 1995a) and as the increase of the error in the Ångström formula for the spectral behavior of AOD.

e. Spectral behavior of τ_λ^A(0.37–4 μm)

There were only isolated cases of investigation into the atmospheric transparency over the ocean in the spectral range above 1 μm. At least, we are aware of two publications by Wolgin et al. (1991) and Villevalde et al. (1994) in the range of 0.46–1.64 μm, related to shipborne investigations in the Norwegian Sea and the Pacific Ocean. We made measurements of τ_λ^A in the spectral range of 0.37–4 μm only in 1995 and 1996. Below we consider the mean spectra for the obtained data.

Figure 14 shows, as expected, that in the longwave range, the spectral dependence of $\tau^A(\lambda)$ changes from power to neutral. For the sake of comparison, the results of other investigations in similar conditions are shown in the same figure. Note that the data obtained in the Dark Sea are close to the values of $\tau^A(\lambda)$ obtained during dust emissions in Senegal (Tanre et al. 1988) and in the south of France (Deuze et al. 1988). The measurements in the Norwegian Sea (curves 1 and 2) were carried out relatively close to land, so the obtained data are intermediate among the spectra of $\tau^A(\lambda)$ obtained in the MO and NC areas.

As noted by many authors, the description of $\tau^A(\lambda)$ by Eq. (11) in the extended wavelength range is not justifiable. In our case, the mean values of the deviation of $\tau^A(\lambda)$ from the power dependence amounts to tens of percent. A more appropriate representation of $\tau^A(\lambda)$ is in the form of the sum of two components related to fine and coarse aerosol fractions:

$$\tau^A(\lambda) = \tau_f + \tau_c = m\lambda^{-n} + \tau_c, \qquad (12)$$

where the parameters m and n have the same meaning as in Eq. (11), but only for fine aerosol. For τ_c, which has neutral spectral behavior, one can use the value of AOD in the range of 4 μm.

The parameters in the modeled dependence (12) calculated by the least squares method enable us to estimate the contribution of fine and coarse aerosol for different regions (Table 6). In particular, the value, $\gamma = (m\lambda^{-n}/\tau_c)$, characterizes redistribution of the effect of two fractions in the wavelength range from 0.37 to 1.06 μm. Judging by the high values of m and γ, the DS area is characterized by a large content of both coarse and fine aerosol. The regions were divided into three groups according to the degree of selectivity of $\tau_f(\lambda)$: minimum values of n are observed in the trade wind zone; intermediate in CI, IC, and NC areas; and the maximum values are in MO area. Insufficient data do not allow us to unambiguously interpret this fact. We can only

TABLE 6. Parameters of the dependence $\tau^A(\lambda)$ [Eq. (12)] and estimate of the contribution of fine and coarse aerosol in the spectral and integral AOD.

	MO	TW	CI	DS	IC	NC
$\tau_c = \tau_4$	0,054	0,157	0,124	0,303	0,071	0,058
m	0,002	0,020	0,016	0,089	0,022	0,027
n	2,83	1.30	1,85	1,30	1,91	2,06
$\gamma_\lambda = \tau_f/\tau_c$ (0.37–1 μm)	0,62–0,03	0,46–0,12	0,81–0,12	1,07–0,27	2,07–0,28	3,61–0,41
τ^*	0,061	0,188	0,157	0,443	0,117	0,120
τ_f^*	0,007	0,031	0,033	0,140	0,046	0,062
τ_f^*/τ_c^*	0,13	0,20	0,27	0,46	0,65	1,06

TABLE 7. Statistics of the parameters of Eq. (13).

	Mean	Std dev	Min	Max	V
τ_c	0.035	0.011	0.019	0.064	0.31
m_0	0.0038	0.0018	0.001	0.008	0.49
n_0	2.18	0.66	0.76	3.15	0.30

suppose that the fine aerosol mode in the clear air of the MO area is most narrow and is shifted to a smaller size.

The spectral behavior of $\tau^A(\lambda)$ in the MO area, as far as the background issues are concerned, is interesting by itself. The fact is that the atmosphere of remote areas loses its regional dependence on the sources (emissions) of continental aerosol and is approximately the same for the whole World Ocean. The investigations in the Pacific and the Indian Oceans (Barteneva et al. 1991; Volgin et al. 1988; Smirnov et al. 1995b) confirm this observation. The mean spectra obtained in the MO area (Fig. 14) shows that $\tau^A(\lambda)$ reaches the neutral dependence significantly earlier. In this case one can estimate the coarse component τ_c from the minimum values of AOD in the shorter wave range ($\tau_c = \tau_{\min}$ in the range from 0.6 to 1 μm). Therefore, in the MO area one can use the total bulk of data (0.37 to 1.06 μm) instead of limited array of data (0.37–4 μm) in order to obtain a dependence of the form of Eq. (12):

$$\tau^A(\lambda) = m_0\lambda^{-n0} + \tau_c. \qquad (13)$$

To determine the spectrum of $\tau^A(\lambda)$ which actually corresponds to the background conditions, rare cases of ''surges'' of the values τ^A in the shortwave range were excluded from the bulk of data, and the statistics of the parameters m_0 and n_0 was calculated (Table 7). From the statistical characteristics one can judge about the content of two main fractions: large marine particles and fine, apparently, sulfate aerosol. One can consider Eq. (13) together with corresponding values of m_0 and n_0 as a few-parameter model of $\tau^A(\lambda)$ for the background oceanic atmosphere.

f. Integral transparency of the atmosphere

Determination of the integral (over spectrum 0.37 to 4 μm) transparency of the atmosphere and the direct radiation S was based on the results of AOD zoning. First, we determined the aerosol transparency component T^A for the separated areas. Then the mean values of columnar water vapor W were selected for the same areas from the long-term data (Tuller 1968), and the transmission functions T^W were calculated. The integral transparency T^Σ was determined at the last stage, taking into account the constant gases. The calculations were carried out for the sun elevation of 30° using the LOWTRAN-7 code by the formulas of the form

$$T^\Sigma = \int S_{0\lambda}T^A_\lambda T^W_\lambda T^X_\lambda T^C_\lambda \, d\lambda \Big/ \int S_{0\lambda}\, d\lambda, \qquad (14)$$

where $S_{0\lambda}$ is the extraterrestrial spectral irradiance.

The mean spectra of τ^A_λ (Table 4) were used to calculate T^A in the range of up to 1 μm; as for the longwave range, the neutral dependence was assumed. The latter is explained by insufficient statistics on τ^A_λ in the IR range. However, it is more important that the effect of aerosol in the IR range decreases, and the transparency T^Σ is mainly determined by the ''water vapor'' component T^W. Thus, the mean distribution of the transparency and direct solar radiation over the Atlantic was obtained (Table 8). It follows from the derived results that due to spatial inhomogeneities of aerosol and the water vapor the value of T^Σ changes by a factor of about 2. The aerosol component plays a more significant role in the variations of T^Σ. The range of T^A is from 0.5 to 0.87, and T^W is from 0.77 to 0.84. Greater variability of T^A is characteristic of both latitudinal and meridional cuts. According to the calculations, a maximum income of direct radiation, 0.82 kW m^{-2}, under average conditions of cloudless atmosphere is observed at temperate latitudes in the midocean areas, and the minimum is in DS areas, 0.452 kW m^{-2}.

One more issue was considered, based on the obtained data. We estimated the effect of fine and coarse aerosol

TABLE 8. Components of the total transparency and direct radiation in different areas (areas in the limits of the latitudinal zone are ordered from west to east).

Climatic zone	Area	W (g cm^{-2})	T^A	T^W	T^Σ	S (W m^{-2})
Temperate latitudes	NC	1,27	0,792	0,840	0,561	767
	MO	1,80	0,872	0,823	0,605	827
	NC	1,65	0,792	0,828	0,553	756
Subtropics	NC	3,35	0,792	0,787	0,526	719
	MO	3,2	0,872	0,790	0,581	794
	CI	2,4	0,796	0,807	0,542	741
Tropical (trade wind) zone	NC	4,2	0,792	0,771	0,516	705
	MO	4,05	0,872	0,774	0,570	779
	TW	3,65	0,683	0,781	0,451	617
	DS	3,3	0,498	0,788	0,331	452
Equatorial latitudes	IC	4,5	0,787	0,767	0,510	697

on the integral AOD of the atmosphere (0.37 to 4 μm, $M = 1$):

$$\tau^* = \tau_f^* + \tau_c^* = -\ln T^A = -\ln\left[\int S_{0\lambda} \exp(-\tau_\lambda^A)\, d\lambda \Big/ \int S_{0\lambda}\, d\lambda\right]. \quad (15)$$

As before, the coarse component $\tau_c^* = \tau_c^*$ was determined from the value of τ_λ^A in the range of 4 μm, and the fine components were calculated from the difference $\tau_f^* = (\tau^* - \tau_c^*)$. The results of calculations showed that coarse aerosol is the main factor that affects the τ^* and the income of direct radiation in the majority of regions (lower part of Table 6). The fine fraction becomes prevalent only in coastal areas at temperate latitudes (NC). In the remote regions of ocean (MO and TW) the contribution in AOD fine aerosol does not exceed 20%.

4. Conclusions

During our research work we developed a multiwave sun photometer, along with algorithms and software, suitable to carry out continuous real-time measurements of the marine atmosphere transparency and AOD in a wide spectral range. The experience of a number of sea expeditions confirmed the efficiency of the chosen approach to the measurement even under most complex conditions—sun irradiation measurements through small and fast-changing cloud breaks, complicated by the ship's rolling and maneuvers.

In this paper, supported by previous results, we have discussed main patterns and regularities in the variability of atmospheric transparency over the ocean. A stress is put on the necessity of regional approach to its properties. The spatial inhomogeneities of τ_λ^A are shown to be primarily caused by different concentration of continental aerosol in the atmosphere: fine aerosol at midlatitudes and coarse aerosol in the Tropics. Based on the results of genetic and sign zoning, we have proposed and substantiated the model for spatial distribution of aerosol atmospheric turbidity over the Atlantic. At temperate latitudes we separated a narrow littoral zone, near-to-continent and the midocean (remote) areas. In the Tropics, we have classified the trade wind zone with the most turbid Dark Sea, and the mixed areas (CI and MS). The equatorial, or the intertropical convergence zone, is situated in the southern part of the investigated area. In this zone, the difference of aerosol characteristics from the neighboring trade wind zone is caused by the peculiarities of meteorological conditions: high humidity, small wind velocity, filtration of Saharan aerosol by cloudiness, and precipitation. The range of variability of $\tau_{0.55}^A$ in the selected areas is from 0.07 to 0.38.

The parameters of empirical dependencies $\tau^A(\lambda)$ determined for the shortwave range provide a qualitative description of the mean spectral behavior of atmospheric AOD and its variability in different regions. The mean values of the parameter α lie in the limits from minimum 0.3 in the trade wind zone to maximum 1.1 near the continents at temperate latitudes. The features of the spectral dependence of $\tau^A(\lambda)$ are considered in the extended wavelength range, and the expedience is noted of its description by the sum of two components related to fine and coarse aerosol. Assessment of the effect of two fractions on the formation of atmospheric AOD shows that coarse aerosol plays predominant role over the greater part of the ocean. The contribution of fine aerosol is prevalent only near the continent at temperate latitudes. Concerning the total atmospheric transparency, the aerosol component T^A is shown to be most subject to variation. The spatial variability of the atmospheric transparency over the Atlantic is characterized by the following mean values (at $Z = 60°$): $T^A = 0.5$–0.87, $T^W = 0.77$–0.84, and $T^\Sigma = 0.33$–0.61.

The quantity of experimental data still remains insufficient to develop qualitative empirical models of aerosol atmospheric turbidity over the ocean which would account for seasonal variations. So we do not claim that our model is complete; we rather see our main goal in the formulation and substantiation of the principles of the ocean zoning, which will allow for systematic analysis of isolated results obtained in different areas. Comparison of the mean characteristics of τ^A and α with the data of other authors gives us ground to consider that our investigations derived the most substantiated estimates of spectral AOD for the central and the North Atlantic.

Acknowledgments. The authors would like to thank academician V. E. Zuev (Institute of Atmospheric Optics, Tomsk, Russia) and the Director of Instituto Canario de Ciencias Marinas (Gran Canaria, Spain), who were heads of the expeditions; A. M. Sagalevitch (Institute of Oceanology, Moscow, Russia); and G. K. Korotaev and N. A. Panteleev (Marine Hydrophysics Institute, Sevastopol, Ukraine), who favored the long-term investigations of the spectral transparency of the atmosphere over the Atlantic ocean. We especially thank L. L. Stowe, P. Clemente-Colon, and A. M. Ignatov (Satellite Research Laboratory, NOAA/NESDIS, Washington D.C.) for the help in the investigations and the financial support of the 1994 expedition.

REFERENCES

Alisov, B. P., and B. V. Poltorays, 1983: *Climatology* (in Russian). MGY, 168 pp.

Ångström, A., 1961: Techniques of determining the turbidity of the atmosphere. *Tellus*, **13,** 214–222.

Barteneva, O. D., L. K. Veselova, G. G. Sakynov, and N. I. Nikitinskaya, 1991: *Atmospheric Transmittance in the Visible and Near IR Spectral Range* (in Russian). Gidrometeoizdat, 224 pp.

Cachorro, V. E., P. Duran, R. Vergaz, and A. M. de Frutos, 1987: Determination of the Ångström turbidity parameters, *Appl. Opt.*, **26,** 3069–3076.

——, ——, ——, and ——, 2000: Measurements of the atmospheric

turbidity of the north-centre continental area in Spain: Spectral aerosol optical depth and Ångström turbidity parameters. *J. Aerosol Sci.,* **31,** 687–702.

Cuomo, V., F. Esposito, G. Pavese, and C. Serio, 1993: Determing Ångström's turbidity coefficients. *Aerosol Sci. Technol.,* **18,** 59–69.

d'Almeida, G. A., P. Koepke, and E. P. Shettle, 1991: *Atmospheric Aerosol: Global Climatology and Radiative Characteristics.* A. Deepak, 561 pp.

Deuze, J. L., C. Devaux, M. Herman, R. Santer, and D. Tanre, 1988: Saharan aerosols over the south of France: Characterization derived from satellite data and ground-based measurements. *J. Appl. Meteor.,* **27,** 680–686.

Ershov, D. M., A. V. Smirnov, and K. S. Shifrin, 1990: Spectral transparency and solar halo in the atmosphere above the ocean. *Izv. Acad. Sci. USSR Atmos. Oceanic Phys. (Engl. transl.),* **26,** 287–292.

Fitzgerald, J. W., 1991: Marine aerosols: A review. *Atmos. Environ.,* **25A,** 533–545.

Flohn, H., 1957: On classification of climatic zones. (in German). *Ertkunde,* **11,** 161–175.

Forgan, B. W., 1988: Bias in a solar constant determination by the Langley method due to structured atmospheric aerosol: Comment. *Appl. Opt.,* **27,** 2546–2548.

——, 1994: General method for calibration of sun photometers. *Appl. Opt.,* **33,** 4841–4850.

——, J. J. DeLuisi, B. B. Hick, and E. N. Rusina, 1994: Report on the measurements of atmospheric turbidity in BARMoN. WMO/TD-No. 603, 77 pp.

Gushin, G. P., 1988: *Methods, Equipment, and Results of Atmospheric Spectral Transmittance Measurements* (in Russian). Gidrometeoizdat, 200 pp.

Halthore, R. N., B. L. Markham, R. A. Ferrare, and T. O. Aro, 1992: Aerosol optical properties over the midcontinental United States. *J. Geophys. Res.,* **97** (D17), 18 769–18 778.

Hansen, J. E., and L. D. Travis, 1974: Light scattering in planetary atmospheres. *Space Sci. Rev.,* **16,** 527.

Herman, B. M., M. A. Box, J. A. Reagan, and C. M. Evans, 1981: Alternative approach to the analysis of solar photometer data. *Appl. Opt.,* **20,** 2925–2928.

Hoppel, W. A., J. W. Fitzgerald, G. M. Frick, and R. E. Larson, 1990: Aerosol size distributions and optical properties found in the marine boundary layer over the Atlantic Ocean. *J. Geophys. Res.,* **95** (D4), 3659–3686.

Hoyningen-Huene, W., and A. Raabe, 1987: Maritime and continental air mass differences in optical aerosol extinction. *Beitr. Phys. Atmos.,* **60,** 81–87.

Ignatov, A. M., I. L. Dergileva, S. M. Sakerin, and D. M. Kabanov, 1993: An algorithm for the sun photometer calibration. *Proc. IGARSS'93,* Tokyo, Japan, Institute of Electrical and Electronics Engineers, 1091–1093.

——, ——, Yu. Ratner, S. Sakerin, and D. Kabanov, 1994: Aerosol optical thickness retrieval from sun photometer measurements. *Proc. IGARSS'94,* Pasadena, CA, Institute of Electrical and Electronics Engineers, 1497–1499.

——, L. L. Stowe, S. M. Sakerin, and G. K. Korotaev, 1995: Validation of NOAA/NESDIS satellite aerosol product over the North Atlantic in 1989. *J. Geophys. Res.,* **100** (D3), 5123–5132.

Kabanov, D. M., and S. M. Sakerin, 1996: Variations of the aerosol optical depth of the atmosphere above Tomsk for number of seasons in 1992–1995. *Atmos. Oceanic Opt.,* **9,** 459–463.

——, and ——, 1997a: About method of atmospheric aerosol optical thickness determination in near-IR spectral range. *Atmos. Oceanic Opt.,* **10,** 540–545.

——, and ——, 1997b: Results of measurements of aerosols optical thickness and moisture content in the atmosphere of central Atlantic. *Atmos. Oceanic Opt.,* **10,** 913–918.

——, ——, A. M. Sytormin, and S. A. Turchinovich, 1993: Wideband solar photometer for a marine atmospheres studies. *Atmos. Oceanic Opt.,* **6,** 270–273.

Kasten, F., 1966: A new table and approximation formula for the relative optical air mass. *Arch. Meteor. Geophys. Bioclimatol.,* **B14,** 206–223.

Kaufman, Y. J., and Coauthors, 1997: Passive remote sensing of tropospheric aerosol and atmospheric correction for the aerosol effect. *J. Geophys. Res.,* **102** (D14), 16 815–16 830.

Kneizys, F. X., E. P. Shettle, W. O. Gallery, J. H. Chetwynd, L. W. Abreu, J. E. A. Selby, S. A. Clough, and R. W. Fenn, 1983: Atmospheric transmittance/radiance: Computer code LOWTRAN-6. Hanscom Air Force Base Tech. Note AFGL-TR-83-0187, 200 pp.

——, ——, L. W. Abreu, J. H. Chetwynd, J. P. Anderson, W. O. Gallery, J. E. A. Selby, and S. A. Clough 1988: Users guide to LOWTRAN-7. Hanscom Air Force Base Tech. Note AFGL-TR-0177, 137 pp.

Kondratyev, K. Y., Ed., 1991: *Aerosol and Climate* (in Russian). Gidrometeoizdat, 541 pp.

——, and O. D. Barteneva, 1976: Aerosol in the ATEP region and its radiative properties (in Russian). *Proc. GGO,* **381,** 67–130.

——, N. I. Moskalenko, and D. V. Pozdnakov, 1983: *Atmospheric Aerosol* (in Russian). Gidrometeoizdat, 224 pp.

Kool, L. V., 1975: Seasonal differences in the resulting wind field in Atlantic. *Meteorological Researches in the Tropical Ocean* (in Russian), Nayka, 85–94.

Korotaev, G., S. Sakerin, A. Ignatov, L. Stowe, and P. McClain, 1993: Sun-photometer observations of aerosol optical thickness over the North Atlantic from a Soviet research vessel for validation of satellite measurements. *J. Atmos. Oceanic Technol.,* **10,** 725–735.

Mishchenko, M. I., I. V. Geogdzhayev, B. Cairns, W. B. Rossov, and A. A. Lacis, 1999: Aerosol retrievals over the ocean by use of channels 1 and 2 AVHRR data: Sensitivity analysis and preliminary results. *Appl. Opt.,* **38,** 7325–7341.

Moorthy, K. K., S. K. Satheesh, and B. V. K. Murthy, 1997: Investigations of marine aerosols over the tropical Indian Ocean. *J. Geophys. Res.,* **102** (D15), 18 827–18 842.

Peterson, J. T., E. C. Flovers, G. J. Berri, C. L. Reynolds, and J. H. Rudisill, 1981: Atmospheric turbidity over central North Carolina. *J. Appl. Meteor.,* **20,** 229–241.

Prospero, J. M., 1979: Mineral sea salt aerosol concentrations in various ocean regions. *J. Geophys. Res.,* **84,** 725–731.

Rao, C. R. N., L. L. Stowe, and E. P. McClain, 1989: Remote sensing of aerosols over the oceans using AVHRR data: Theory, practice and applications. *Int. J. Remote Sens.,* **10,** 743–749.

Reagan, J. A., L. W. Thomason, B. M. Herman, and J. M. Palmer, 1986: Assessment of atmospheric limitations on the determination of the solar spectral constant from ground-based spectroradiometer measurements. *IEEE Trans. Geosci. Remote Sens.,* **GE24** (2), 258–266.

——, K. J. Thome, and B. M. Herman, 1992: A simple instrument and technique for measuring columnar water vapor via near-IR differential solar transmission measurements. *IEEE Trans. Geosci. Remote Sens.,* **30,** 825–831.

Reddy, P. J., F. W. Kreiner, J. J. DeLuise, and Y. Kim, 1990: Aerosol optical depths over the Atlantic derived from shipboard sunphotometer observations during the 1988 Global Change Expedition. *Global Biogeochem. Cycles,* **4,** 225–240.

Roll, H. U., 1965: *Physics of Marine Atmosphere.* Academic Press, 426 pp.

Sakerin, S. M., and D. M. Kabanov, 1997: Taking into account optical airmasses of atmospheric components in the method of solar photometry at big zenith angles of observations. *Extended Abstracts, Fourth Symp. on Atmospheric and Ocean Optics,* Tomsk, Russia, Institute of Atmospheric Optics, 155–156.

——, S. V. Afonin, T. A. Eryomina, A. M. Ignatov, and D. M. Kabanov, 1991: General characterization and statistical parameters of the atmospheric spectral transmission in some regions of the Atlantic. *Atmos. Oceanic Opt.,* **4,** 504–510.

——, I. L. Dergileva, A. M. Ignatov, and D. M. Kabanov, 1993: Enhancement of the turbidity of the atmosphere over the Atlantic

in the post Mt. Pinatubo eruption period. *Atmos. Oceanic Opt.,* **6,** 707–714.

——, D. M. Kabanov, and V. V. Polkin, 1995: Optical investigations of atmosphere during the 35th voyage of the research vessel *Acad. Mstislav Keldysh. Atmos. Oceanic Opt.,* **8,** 981–988.

——, ——, and S. A. Turchinovich, 1996: Instrumentation for radiation investigation. *Atmos. Oceanic Opt.,* **9,** 1046–1052.

Samoilenko, V. S., Ed., 1983: *Variability of Physical Fields in the Atmosphere over the Ocean* (in Russian). Nayka, 168 pp.

Satheesh, S. K., K. K. Moorthy, and B. V. K. Murthy, 1998: Spatial gradient in aerosol characteristics over the Arabian Sea and Indian Ocean. *J. Geophys. Res.,* **103** (D20), 26 183–26 192.

Shaw, G. E., J. A. Reagan, and B. M. Herman, 1973: Investigation of atmospheric extinction using direct solar radiation measurements made with a multiple wavelength radiometer. *J. Appl. Meteor.,* **12,** 374–380.

Shifrin, K. S., O. A. Yershov, V. M. Volgin, and A. M. Kokorin, 1980: Maritime aerosol studies based on coastal observations data. *Izv. Acad. Sci. USSR Atmos. Oceanic Phys. (Engl. transl.),* **16,** 166–170.

Shiobara, M., J. D. Spinhirne, A. Uchiyama, and S. Asano, 1996: Optical depth measurement of aerosol, cloud, and water vapor using sun photometers during FIRE Cirrus IFO II. *J. Appl. Meteor.,* **35,** 36–46.

Smirnov, A. V., Y. V. Villevalde, N. T. O'Neill, A. Royer, and A. Tarussov, 1995a: Aerosol optical depth over the oceans: Analysis in term of synoptic air mass types. *J. Geophys. Res.,* **100** (D8), 16 639–16 650.

——, O. Yershov, and Y. Villevalde, 1995b: Measurement of aerosol optical depth in the Atlantic Ocean and Mediterranean Sea. *Proc. Eur. Symp. Sattel. Remote Sens. II,* **2582,** 203–214.

Soufflet, V., C. Devaux, and D. Tanre, 1992: Modified Langley plot method for measuring the spectral aerosol optical thickness and its daily variations. *Appl. Opt.,* **31,** 2154–2162.

Spinhirne, J. D., M. G. Strange, and L. R. Blaine, 1985: Solar infrared photometer. *J. Atmos. Oceanic Technol.,* **2,** 264–267.

Swap, R., S. Ulanski, M. Cobbet, and M. Garstang, 1996: Temporal and spatial characteristics of Saharan dust outbreaks. *J. Geophys. Res.,* **101** (D2), 4205–4220.

Tanre, D., P. Y. Deshamps, C. Devaux, and M. Herman, 1988: Estimation of Saharan aerosol optical thickness from blurring effects in thematic mapper data. *J. Geophys. Res.* **93** (D12), 15 955–15 964.

——, B. N. Holben, and Y. J. Kaufman, 1992: Atmospheric correction algorithm for NOAA/AVHRR products: Theory and application. *IEEE Trans. Geosci. Remote Sens.,* **30,** 231–248.

——, Y. J. Kaufman, M. Herman, and S. Mattoo, 1997: Remote sensing of aerosol properties over oceans using the MODIS/EOS spectral radiances. *J. Geophys. Res.,* **102** (D14), 16 971–16 988.

Tomasi, C., and F. Prodi, 1982: Measurement of atmospheric turbidity and vertical mass loading of particulate matter in marine environments (Red Sea, Indian Ocean, and Somalian coast). *J. Geophys. Res.,* **87** (C2), 1279–1286.

Tuller, S. E., 1968: World distribution of mean monthly and annual precipitable water. *Mon. Wea. Rev.,* **96,** 785–797.

Villevalde, Y. V., A. V. Smirnov, N. T. O'Neill, S. P. Smyshlyaev, and V. V. Yakovlev, 1994 Measurement of aerosol optical depth in the Pacific Ocean and the North Atlantic. *J. Geophys. Res.,* **99,** 20 983–20 988.

Volgin, V. M., O. A. Yershov, A. V. Smirnov, and K. S. Shifrin, 1988: Optical depth of aerosol in typical sea areas. *Izv. Acad. Sci. USSR Atmos. Oceanic Phys. (Engl. transl.),* **24,** 772–777.

Wolgin, W. M., W. F. Radionov, and U. Leiterer, 1991: Varying the optical characteristics of the North Atlantic atmosphere (in German). *Z. Meteor.,* **41,** 267–272.

Yershov, O. A., A. V. Smirnov, K. S. Shifrin, 1990: Spectral transparency and solar halo in the atmosphere above the ocean. *Izv. Acad. Sci. USSR Atmos. Oceanic Phys. (Engl. transl.),* **26,** 287–292.

Zyev, V. E., S. M. Sakerin, and D. M. Kabanov, 1997: Variation of aerosol optical thickness and moisture content of the atmosphere in the area of Canary Islands. *Proc. Ocean Opt. XIII,* **2963,** 821–825.